

1
2 **Integrated *in silico* and *Drosophila* cancer model platform captures previously un-**
3 **appreciated chemicals perturbing a kinase network**

4
5 Peter Man-Un Ung^{1†}, Masahiro Sonoshita^{2†}, Alex P. Scopton³, Arvin C. Dar³, Ross L.
6 Cagan^{2*}, Avner Schlessinger^{1*}

7
8 ¹*Department of Pharmacological Sciences, Icahn School of Medicine at Mount Sinai, New*
9 *York, NY, 10029.*

10 ²*Department of Cell, Developmental and Regenerative Biology, Icahn School of Medicine*
11 *at Mount Sinai, New York, NY 10029.*

12 ³*Department of Oncological Sciences, Icahn School of Medicine at Mount Sinai, New*
13 *York, NY 10029.*

14
15
16 * Corresponding authors. E-mail:

17 ross.cagan@mssm.edu

18 avner.schlessinger@mssm.edu

19 † These authors contributed equally to this work.

20 **ABSTRACT**

21 *Drosophila* provides an inexpensive and quantitative platform for measuring whole animal
22 drug response. A complementary approach is virtual screening, where chemical libraries
23 can be efficiently screened against protein target(s). Here, we present a unique discovery
24 platform integrating structure-based modeling with *Drosophila* biology and organic syn-
25 thesis. We demonstrate this platform by developing chemicals targeting a *Drosophila*
26 model of Medullary Thyroid Cancer (MTC) with disease-promoting kinase network acti-
27 vated by mutant dRet^{M955T}. Structural models for kinases relevant to MTC were generated
28 for virtually screening to identify initial hits that were dissimilar to known kinase inhibitors
29 yet suppressed dRet^{M955T}-induced oncogenicity. We then combined features from the hits
30 and known inhibitors to create a ‘hybrid’ molecule with improved dRet^{M955T} phenotypic
31 outcome. Our platform provides a framework to efficiently explore novel chemical spaces,
32 develop compounds outside of the current inhibitor chemical space, and “correct” cancer-
33 causing signaling networks to improve disease prognosis while minimizing whole body
34 toxicity.

35

36 Protein kinases play a key role in cell signaling and disease networks and make
37 up major therapeutic targets. The limited capacity to test large number of compounds
38 exploring diverse chemical scaffolds, coupled with the low translatability of *in vitro* kinase
39 inhibition into whole animal efficacy, effectively constrain the chemical space of the known
40 kinase inhibitors (KIs). Thus, obtaining optimal KIs at clinically relevant therapeutic levels
41 is challenging, despite extensive academic and industry effort.

42 To expand the number of kinase inhibitors, a variety of platforms have recently
43 emerged as useful tools for compound screening. *Drosophila melanogaster* (fruit fly) pro-
44 vides an inexpensive and efficient biological platform for cancer drug screening, capturing
45 clinically relevant compounds^{1, 2, 3}. For example, *Drosophila* was used to help validate
46 vandetanib as a useful treatment for medullary thyroid cancer⁴ (MTC). As a screening
47 platform, *Drosophila* offers several advantages: First, flies and humans share similar ki-
48 nome and kinase-driven signaling pathways⁵, facilitating the use of flies to predict drug
49 response in humans^{1, 6}. Second, the ease of breeding and the short (~10 day) life cycle
50 of *Drosophila* make it possible to carry out efficient mid-throughput chemical screening in
51 a biological system. Third, the screening readout provides a quantitative animal-based
52 measurement of structure-activity relationships (SAR), and further provides information
53 on the therapeutic potential or toxicity of the tested compounds: measurable parameters
54 include survival and multiple phenotypic indicators that depend on kinase activity.

55 One key limitation of *Drosophila*-based mid-throughput screening platform is that
56 it cannot explore very large chemical libraries⁷, such as the ZINC library which has over
57 750 million purchasable compounds⁸. In contrast, structure-based virtual screening is a
58 fast and inexpensive computational method that can screen large compound libraries, a
59 useful approach to identify unique chemical probes⁹. If the structure of the protein is un-
60 known, virtual screening can be performed against the homology models of the target
61 constructed based on experimentally determined structures. However, the automated
62 construction of homology models—with sufficient accuracy for virtual screening for multi-
63 ple targets simultaneously and the application of molecular docking to signaling net-
64 works—remains challenging in particular for highly dynamic targets such as kinases^{10, 11}
65 and would benefit from a readily accessible whole animal platform.

66 RET is a receptor tyrosine kinase associated with multiple roles in development
67 and homeostasis. Activation of RET by the mutation M918T (analogous to *Drosophila*
68 M955T) is associated with MTC^{12, 13}. Transgenic *Drosophila* expressing the dRet^{M955T}
69 isoform show key aspects of transformation, including proliferation and some aspects of
70 metastasis^{6, 14}. Genetic modifier screens with dRet^{M955T} flies led to the identification of
71 multiple RET pathway genetic ‘suppressors’ and ‘enhancers’, loci that when reduced in
72 activity improve or worsen the disease phenotype, respectively. These functional media-
73 tors of RET-dependent transformation include members of the Ras/ERK and PI3K path-
74 ways as well as regulators of metastasis such as SRC^{6, 15}.

75 Oral administration of the FDA approved, structurally related multi-kinase inhibitor
76 analogs sorafenib and regorafenib, along with additional structural analogs, partially res-
77 cued dRet^{M955T}-induced oncogenicity in *Drosophila*^{1, 15}. Sorafenib class inhibitors are
78 classified as ‘type-II’ KIs that bind the kinase domain in its inactive state¹⁶, a conforma-
79 tional state regulated by the aspartate-phenylalanine-glycine (DFG)-motif^{17, 18} (Fig. 1A)^{17,}
80 ^{18 17, 18 17, 18 17, 18 17, 18 17, 18}. In the inactive, ‘DFG-out’ conformational state the directions of
81 DFG-Asp and DFG-Phe ‘flip’, vacating a pocket previously occupied by DFG-Phe (‘DFG-
82 pocket’) that modulates binding to type-II inhibitors. A key challenge of targeting kinases
83 in the DFG-out conformation with structure-based virtual screening is that few kinase
84 structures have been reported with the DFG-out conformation¹⁹. We have recently devel-
85 oped DFGmodel¹⁰, a computational method for modeling kinases in DFG-out confor-
86 mations. This method informed the mechanism of clinically relevant multi-kinase inhibitors
87 that target the MTC network¹⁵.

88 In this study, we report the development of an integrated platform (Fig. 2) that
89 combines (i) computational modeling of kinases in their inactive state plus massive multi-
90 target virtual screenings with (ii) whole animal *Drosophila* assays to discover previously
91 unappreciated chemicals that perturb the RET-dependent transformation. Furthermore,
92 we leverage these insights to create a novel ‘hybrid’ molecule with unique chemical struc-
93 ture and biological efficacy. Finally, we discuss the relevance of this approach to expedite
94 the discovery of novel chemical scaffolds targeting disease networks.

95

96 RESULTS

97 **Target selection from fly genetic screen and structural analysis.** In transgenic
98 *patched-GAL4;UAS-dRet^{M955T}* (*ptc>dRet^{M955T}*) flies, the *ptc* promoter drives expression
99 of an oncogenic isoform of *Drosophila* Ret in multiple tissues; the result is lethality prior
100 to adult eclosion^{1, 15}. We previously used this and similar fly MTC models in genetic
101 screens to identify 104 kinases that mediate *dRet^{M955T}*-mediated transformation¹⁵ (Figs.
102 1B, 2A, S1).

103 To narrow this list, we prioritized candidates based on two considerations: (i) phar-
104 macological relevance – kinases downstream of RET signaling were prioritized due to
105 their established functional role^{6, 20}; (ii) structural coverage – kinases with known DFG-
106 out structures or those that can be modeled with sufficient accuracy in this conformation
107 were further investigated¹⁰. Atypical kinases (e.g., mTOR and eEF2K) and members of
108 the RGC family were excluded as they have diverse sequence and structure features that
109 limit our ability to generate accurate homology models. Applying these criteria to our ge-
110 netic modifier list, we focused on targeting four key kinase targets: RET (receptor tyrosine
111 kinase), SRC (tyrosine kinase), BRAF (tyrosine kinase-like), and p70-S6K (AGC family).

112 **Modeling kinases in DFG-out conformation.** Description of the various conformations
113 adopted by the kinases during activation and inhibition is needed for rationally designing
114 novel, conformation-specific inhibitors. Therefore, our approach was to perform massive
115 structure-based virtual screenings of purchasable compound libraries against multiple
116 models with DFG-out conformation; our goal was to capture putative multi-target type-II
117 KIs that target one or more prioritized kinases.

118 The structure of two of the kinases identified in our *dRet^{M955T}* model—BRAF and
119 SRC—have been solved in the DFG-out conformation; the DFG-out structures of RET
120 and p70-S6K have not been reported. We therefore generated DFG-out models using
121 DFGmodel, a computational tool that generates homology models of kinase in DFG-out
122 conformation through multiple-template modeling that samples a range of relevant con-
123 formations¹⁰. These models enrich known type-II inhibitors among a diverse set of non-
124 type-II KIs found in PDB with accuracy similar to or better than that obtained for experi-
125 mentally determined structures and provides approximation for binding site flexibility¹⁰.

126 For example, in a recent application of DFGmodel, models generated by this method were
127 used in parallel with medicinal chemistry to optimize clinically relevant compounds that
128 are based on the established kinase inhibitor sorafenib¹⁵. Conversely, in this study, mod-
129 els generated by DFGmodel are used to develop compounds that are outside of the cur-
130 rent kinase inhibitor chemical space.

131 To guide multi-target inhibitor discovery, we first compared the DFG-out models of
132 the kinases, identifying key similarities and differences in physicochemical properties
133 among their inhibitor-binding sites. First, we noted that the prioritized targets RET, BRAF,
134 p70-S6K, and SRC present negative electrostatic potential on the DFG-pocket surface,
135 while many non-targets such as ERK have positive electrostatic potential (Fig. 3A). This
136 difference may partially explain the partial selectivity of type-II inhibitors (e.g., sorafenib)
137 toward our prioritized targets but not on electrostatic positive kinases such as ERK. Se-
138 cond, RET and SRC have large DFG-pocket volumes (163 Å³, 196 Å³); p70-S6K and
139 BRAF have moderately large pockets (158 Å³, 136 Å³). In contrast, ERK has a small DFG-
140 pocket (113 Å³) (Fig. 3B). We used this size difference to computationally select for ki-
141 nases with larger DFG-pockets (e.g., RET, SRC) while excluding kinases with smaller
142 DFG-pockets (e.g., ERK).

143 **Virtual screening against MTC pathway.** We performed virtual screening against mul-
144 tiple DFG-out models of MTC targets to identify putative small molecules that modulate
145 the disease network (Fig. 2C). We docked a purchasable lead-like library from the ZINC
146 database²¹ (2.2 millions compounds) against 10 DFG-out models for each kinase target,
147 yielding over 88 million total docking poses. To combine the screening results, a two-step
148 consensus approach was used. In the first step, compounds that ranked in the top 10%
149 in 5 or more of the 10 models of each kinase were selected, resulting in approximately
150 2,000 compounds per kinase. In the second step, compounds that ranked in the top 25%
151 in at least 3 of 4 targets were selected, resulting in 247 compounds. For comparison,
152 sorafenib, an inhibitor that rescues *ptc>dRet*^{M955T} flies, would rank eighth in this consen-
153 sus docking result. From these consensus compounds, eight commercially available com-
154 pounds were purchased to test their ability to rescue *ptc>dRet*^{M955T} flies (Table S1). These
155 compounds were selected based on their interactions with key elements of the “ensem-
156 ble” of targets’ binding sites, with the emphasis on the conserved glutamate in αC-helix,

157 the amide backbone of DFG-aspartate, and if present, the amide backbone of the hinge
158 region (Fig. S3).

159 **Testing candidates in *ptc>dRet*^{M955T} fly viability assay.** Transgenic *ptc>dRet*^{M955T} flies
160 express the oncogenic *Drosophila* dRet^{M955T} isoform in several tissues in the developing
161 fly, leading to transformation of dRet^{M955T} tissues^{6, 14}. As a result, *ptc>dRet*^{M955T} flies ex-
162 hibited 0% adult viability when cultured at 25°C, providing a quantitative ‘rescue-from-
163 lethality’ assay to test drug efficacy^{1, 15}. Compounds were fed at the highest accessible
164 concentrations (see Experimental Procedures). We used sorafenib as a positive control,
165 as it previously demonstrated the highest level of rescue among FDA-approved KIs in
166 *ptc>dRet*^{M955T} flies¹⁵. Similar to our previous results, feeding *ptc>dRet*^{M955T} larvae soraf-
167 enib (200 µM) improved overall viability to 3-4% adult survival ($P < 0.05$).

168 We used this rescue-from-lethality assay to test the efficacy of the eight com-
169 pounds identified through virtual screening (Figs. 4B, 5B). When fed orally, two unique
170 compounds, **1** and **2** (Table S2), rescued a small fraction of *ptc>dRet*^{M955T} flies to adult-
171 hood (Figs. 4A and 5A) and did not affect the body size of the larvae and pupae, a metrics
172 for comparing food intake, of *ptc>dRet*^{M955T} flies when compared to the wild-type. At the
173 maximum final concentration in fly food (100 µM), **1** rescued 1% ($P < 0.05$) *ptc>dRet*^{M955T}
174 flies to adulthood as compared to 3-4% rescue by sorafenib at 200 µM (Fig. 4A). **1** is
175 characterized by the 3-phenyl-(1*H*)-1,2,4-triazole moiety (Fig. 4B). **2**, characterized by the
176 1*H*-indole-2-carboxamide moiety, improved *ptc>dRet*^{M955T} fly viability to an average of 1%
177 ($P < 0.05$) when tested at 25-400 µM (Fig. 5A,B).

178 **Confirmation of novel chemical scaffolds.** To validate the chemical scaffolds identified
179 in our initial *Drosophila*-based chemical genetic screening, we conducted a ligand-based
180 chemical similarity search in the updated ZINC⁸ to identify analogs of **1** and **2**. For com-
181 pound **1**, we retrieved five compounds that share the 3-phenyl-(1*H*)-1,2,4-triazole feature
182 and have docking poses similar to **1**. Our *ptc>dRet*^{M955T} screen confirmed two active com-
183 pounds, **1-1** and **1-2** (Table S2; Fig. 4A, 4B). **1-1** outperformed **1** slightly in *ptc>dRet*^{M955T}
184 fly rescue at similar concentrations (4%; $P < 0.05$). Conversely, **1-2** was tested at higher
185 concentrations (50 and 200 µM) but did not result in better efficacy ($P < 0.05$).

186 The docking poses of **1-1** and **1-2** resemble the proposed docking pose of **1** (Fig.
187 4B), which has a typical DFG-out-specific, type-II KI binding pose and is predicted to oc-
188 cupy the DFG-pocket with the terminal phenyl moiety. The 1,2,4-triazole moiety, resem-
189 bles the urea moiety found in sorafenib (Fig. 1A), forms favorable hydrogen bonds with
190 the side chain of the conserved α C-helix glutamate residue and the backbone amide of
191 the DFG-Aspartate. In addition, this series of compounds are smaller and shorter (MW <
192 360) than the fully developed type-II KIs (MW > 450) such as sorafenib, as they lack an
193 optimized moiety that interacts with the hinge region of the ligand-binding site (Fig. 4C).

194 Compound **1-2** differs from **1** and **1-1** structurally and was less effective in rescuing
195 *ptc>dRet^{M955T}* flies, even though it was tested at higher concentrations (Fig. 4A). While **1**
196 and **1-1** have an (1*H*)-1,2,4-triazole moiety, **1-2** has an 1,2,4-oxadiazol-5-amine moiety,
197 where the (1*H*)-nitrogen is replaced by an oxygen. This modification distinguishes **1-2**
198 from **1** and **1-1** in their interaction preference: **1-2** loses a hydrogen bond donor due to
199 the nitrogen-to-oxygen substitution, while the electronegative oxygen introduces an unfa-
200 vorable electrostatic repulsion to the carboxylate sidechain of the conserved α C-helix glu-
201 tamate (Fig. 4C, **1-2** insert).

202 Co-administering sorafenib with **1** and **1-1** led to synergistic improvement of
203 *ptc>dRet^{M955T}* fly viability (Fig. 4A). Individually, 200 μ M of sorafenib and 100 μ M of **1**
204 rescued 3% and 1% of *ptc>dRet^{M955T}* flies to adulthood, respectively. Co-administering
205 the two compounds rescued 6% of *ptc>dRet^{M955T}* flies to adulthood ($P < 0.05$). Similarly,
206 co-administering sorafenib and 100 μ M of **1-1** rescued 8% of *ptc>dRet^{M955T}* flies ($P <$
207 0.05). In contrast, co-administering 200 μ M of sorafenib and 200 μ M of **1-2** did not im-
208 prove fly viability. As **1-2** only weakly rescued *ptc>dRet^{M955T}* flies and showed no synergy
209 with sorafenib, we did not pursue this hit any further.

210 We examined the kinase inhibition profile (DiscoverX) of **1** against a subset of the
211 human protein kinome (Table 1). At 50 μ M, **1** did not appreciably inhibit SRC, BRAF, or
212 S6K1, while it demonstrated weak activity against wild-type RET and moderate activity
213 against the oncogenic isoform RET^{M918T}. Of note, **1** inhibited other cancer-related targets
214 such as FLT3 (Table 1), which activates the Ras/ERK signaling pathway²².

215 **1** also showed activity against aspects of transformation and metastasis in the fly.
216 In the mature larva, the *ptc* promoter is active in epithelial cells in a stripe pattern in the
217 midline of the developing wing epithelium (Fig. 4C; wing disc). *ptc*-driven dRet activates
218 multiple signaling pathways, promoting proliferation, epithelial-to-mesenchymal transition
219 (EMT), and invasion of dRet^{M955T}-expressing cells beyond the *ptc* domain¹⁴ (Fig. 4C).
220 Similar to sorafenib, oral administration of **1** blocked the invasion of dRet^{M955T}-expressing
221 cells into the surrounding wing epithelium (Fig. 4B).

222 At lower dosage (25 μM), compound **2** weakly rescued *ptc>dRet*^{M955T} flies (1%; *P*
223 < 0.05) (Fig. 5A). Unlike **1**, **2** did not act synergistically with sorafenib. This difference was
224 confirmed by the kinase inhibition profile of **2** (Table 2), in which it has stronger inhibition
225 of RET and RET^{M918T}, but loses the inhibition of FLT3, two key differences between the
226 kinase inhibition profiles of **1** and **2**.

227 Through a chemical similarity search of the ZINC database, we identified five com-
228 pounds that share the 1*H*-indole-2-carboxamide moiety with docking poses similar to that
229 of **2** (Fig. 5B, 5C; Table S2), and confirmed all five analogs were able to improve the
230 viability of *ptc>dRet*^{M955T} flies (Fig. 5A), albeit with weak efficacy (some have *P*-value
231 above 0.05). At low dose (10 μM), **2-1** showed improved efficacy in rescuing
232 *ptc>dRet*^{M955T} flies relative to **2** and had similar efficacy as sorafenib at 200 μM. However,
233 **2-1** showed poor solubility, limiting its usefulness as lead compound. **2-3** was also more
234 efficacious than **2** and displayed better solubility in both DMSO and water than **2-1**; it also
235 has the *N*-phenylacetamide moiety as a linker group, a common linker feature found in
236 type-II KIs such as imatinib. Compound **2-3** displayed a different inhibition profile than **1**
237 and **2** (Table 2): it strongly inhibits FLT3 and PDGFRB, though is weak against both RET
238 and RET^{M918T} and does not inhibit SRC.

239 **Improving efficacy through compound hybridization.** Interestingly, the chemical scaf-
240 folds of our newly identified active compounds are not associated with inhibition of protein
241 kinases, as the analysis with SEA search²³ — which relates ligand chemical similarity of
242 ligands to protein pharmacology — suggests. However, they provide rescue of
243 *ptc>dRet*^{M955T} flies similar to that of sorafenib and regorafenib¹⁵. The docking poses of
244 these compounds suggest a less-than-optimal interaction with the hinge region of protein

245 kinases, a common feature of most KIs. Furthermore, the relatively low molecular weight
246 (~350 g/mol) of these lead-like compounds provides a window for conducting lead opti-
247 mization with medicinal chemistry. Hence, we sought to improve the efficacy of our com-
248 putationally derived leads by installing a hinge-binding moiety found in known type-II KIs
249 such as sorafenib.

250 We took into consideration the docking poses and phenotypic results of the known
251 type-II kinase inhibitors (sorafenib and AD80¹) and lead compounds, as well as the syn-
252 thetic accessibility and the novelty of the putative hybrid compounds, even if they do not
253 dock optimally to our intended kinase targets. We focused on the functionalization of **2/2-**
254 **3** based on these observations: 1) their 1*H*-indole moiety docks uniquely into the DFG-
255 pocket and with the potential to interact with the α C-helix glutamate (Fig. 5C), 2) their 1*H*-
256 indole-2-carboxamide moiety resembles the urea linker that is commonly found in type-II
257 KIs such as sorafenib (Fig. 6A; blue box), and 3) the *N*-phenylcarboxamide moiety of **2-3**
258 is a common linker between the hinge-binding and the DFG-pocket moieties of type-II
259 KIs, e.g. imatinib (Fig. 6A; grey box), while the *N*-(piperidin-4-yl)carboxamide moiety of **2**
260 is not a common linker, and 4) docking pose of **2/3**'s 1*H*-indole moiety overlaps with the
261 trifluoromethylphenyl moiety of sorafenib/AD80. We performed a fragment exchange at
262 the carboxamide position by combining the 1*H*-indole-2-carboxamide moiety of **2/2-3** with
263 the hinge-binding moiety of sorafenib and of AD80, a multi-kinase inhibitor that has shown
264 promise in MTC treatment¹, to create **3** and **4**, respectively (Fig. 6B).

265 Oral administration of **3** and **4** to *ptc>dRet*^{M955T} flies demonstrated that the efficacy
266 of **4** was low with only 3% rescue, while **3** demonstrated much improved efficacy with
267 15% rescue (Fig. 6C; $P < 0.05$), significantly higher rescue than the parent compound
268 **2/2-3** and sorafenib. Additionally, **3** suppressed the invasion/migration of *dRet*^{M955T}-ex-
269 pressing cells in the wing epithelium (Fig. 6D), further confirming its efficacy against
270 *dRet*^{M955T}-induced oncogenicity. The kinase inhibition profile of **3** (Table 3) resembles
271 that of the parent compound **2-3** (Table 2) with at least two notable exceptions: **3** inhibits
272 CSF1R, PDGFRB, and FLT3, all are receptor tyrosine kinases and orthologs of *Drosophi-*
273 *ila* Pvr that activate the Ras/ERK signaling pathway²⁴ and play key roles in SRC activation

274 and tumor progression; and the inhibition of Aurora kinases AURKB and AURKC (*Dro-*
275 *sophila* ortholog *aurA* or *aurB*). Of note, although **4** did not improve the viability of
276 *ptc>dRet^{M955T}* flies, it shares chemical similarity to several known type-I1/2 kinase inhibi-
277 tors that have the common adenine moiety and a related indole moiety. This group of
278 inhibitors was shown to inhibit other related kinases, increasing our confidence in the
279 relevance of this chemical space for kinase pathway modulation²⁵.

280 DISCUSSION

281 ***Integrated discovery pipeline.*** This study demonstrates the utility of an integrated plat-
282 form that combines *Drosophila* genetics, computational structural biology, and chemical
283 synthesis to enrich for the discovery of useful chemical tools in an established *Drosophila*
284 MTC model (Fig. 2). We have previously shown that *Drosophila* can provide a unique
285 entry point for drug development, by capturing subtle structural changes in lead com-
286 pounds that are often missed by cellular or biochemical assays. Here we refine this ap-
287 proach by iteratively combining experimental testing with computational modeling. Over-
288 all, a key strength of the combined approach is its ability to rapidly and in a cost-effective
289 manner test chemically unique, purchasable compounds with our fly models; this platform
290 allowed us to quickly confirm the *in situ* relevance of active chemotypes through iterations
291 of computational modeling, synthetic chemistry, and phenotypic testing in the fly. We ex-
292 pect this integrated pipeline is generally applicable to kinase networks associated with
293 other diseases⁷.

294 ***DFG-out modeling approach.*** DFGmodel is a recent computational development that
295 generates models of kinases in their inactive, DFG-out conformation for rational design
296 of type-II KIs¹⁰. In a recent study, models generated by DFGmodel were used to guide
297 the optimization of the drug sorafenib, to target a new disease space¹⁵. Here, we demon-
298 strated a successful application of DFGmodel to explore compounds that are not appre-
299 ciated as kinase inhibitors. For each kinase target, DFGmodel uses multiple experimen-
300 tally determined structures as modeling templates and generates multiple homology mod-
301 els. Thus, this method samples a large fraction of the DFG-out conformational space dur-
302 ing the model construction, which enables us to account for the flexibility of the binding
303 site during virtual screening²⁶. Notably, DFG-out models capture key features that are
304 important for protein-ligand interactions in multiple kinases simultaneously, providing a
305 framework for rationalizing activity of known inhibitors and developing unique KIs that
306 target a signaling pathway. For example, our results suggest that the electrostatic poten-
307 tial within the DFG-pocket is a key feature for inhibitor selectivity: ERK has an inverse
308 electrostatic potential in the DFG-pocket than that of the target kinases such as RET and

309 BRAF (Fig. 3), which may explain the insensitivity of ERK toward inhibitors such as so-
310 rafenib.

311 **Identification of biologically active compounds.** Most clinically approved KIs are inef-
312 fective against MTC; the most effective inhibitors, sorafenib and regorafenib, show limited
313 efficacy in the *ptc>dRet^{M955T}* fly model, rescuing 3-4% at 200 μM ¹⁵. Despite considerable
314 academic and industry effort, the known chemical space of kinase inhibitors is limited⁷.
315 For example, sorafenib and regorafenib differ in only one non-hydrogen atom. Through
316 structure-based virtual screening against multiple kinase targets in a disease pathway,
317 we discovered chemically unique compounds (Table S2) with an ability to rescue
318 *ptc>dRet^{M955T}* viability that is similar to the most effective FDA-approved drug sorafenib
319 (Figs. 4 and 5).

320 Importantly, our data indicates that these compounds act through key cancer net-
321 works. For example, compounds **1**, **2**, **2-3** and **3** all have shown the ability to suppress
322 invasion of *ptc>dRet^{M955T}* cells in the wing epithelium. Previous works demonstrated that
323 wing cell invasion is controlled by SRC^{15, 27}, which acts by controlling E-cadherin and
324 Matrix Metalloproteases (MMPs). Of note, **1**, **2**, **2-3** and **3** each show significant activity
325 against orthologs of *Drosophila* Pvr, a key regulator of Src: all show significant activity
326 against human FLT3, while **3** shows additional activity against Pvr orthologs CSF1R and
327 PDGFRB. In addition to being orthologs of Pvr, FLT3, CSF1R, and PDGFRB similarly can
328 activate SRC²⁸. We propose that this activity against regulators of SRC account for the
329 ability of **1**, **2**, **2-3** and **3** to suppress invasion, a key first step in tumor metastasis. Other
330 activities, for example, **3**'s inhibition of Aurora kinases — required for proliferation during
331 tumor progression²⁹ — likely also contributes. Indeed, AURK inhibitors are known to be
332 active against MTC^{30, 31} and synergy between AURKs and FLT3 is currently being ex-
333 plored clinically through a number of dual-AURKB/FLT3 inhibitors^{32 33}.

334 **Recombination of building blocks for future inhibitors.** Though the new tool com-
335 pounds **1** and **2** may not be sufficiently potent to serve as therapeutics, they reveal diverse
336 fragment-like pharmacophores that serve as starting points for an exploration of new
337 chemical space. These pharmacophores can be further optimized by combining with well-
338 developed chemotypes that are known to interact with kinase binding sites (e.g., the hinge

339 binding region) to form more efficacious chemical probes; this provides a key second step
340 towards building effective compounds. For example, **2** and **2-3** include an 1*H*-indole moi-
341 ety capable of occupying the DFG-pocket of protein kinases from different families and a
342 carboxamide group commonly found in type-II KIs (Fig. 6A). Guided by the docking poses
343 of these compounds, the 1*H*-indole-2-carboxamide group was combined with an opti-
344 mized hinge-binding moiety from sorafenib, to form a significantly more efficacious com-
345 pound (i.e., **3**). As indicated in the kinase inhibition profile of **3** (Table 3), it shares part of
346 the target set of its constituents **2** and **2-3**.

347 In summary, we demonstrate the potential of combining chemical modeling with
348 *Drosophila* genetics to rapidly and efficiently explore novel chemical space. This provides
349 an accessible and cost-effective platform that can be applied to a broad palette of dis-
350 eases that can be modeled in *Drosophila*. Combining the strengths of these two high-
351 throughput approaches opens the opportunity to develop novel tool and lead compounds
352 that are effective in the context of the whole animal.

353

354 **EXPERIMENTAL PROCEDURES**

355 **DFG-out models.** Models of kinase targets (human RET, SRC, BRAF, S6K1) in the DFG-
356 out conformation were generated using DFGmodel¹⁰. Briefly, the method takes a DFG-in
357 structure or the sequence of the protein kinase as input. DFG-model relies on a manually
358 curated alignment between the target kinase and multiple structures representing unique
359 DFG-out conformations. It calls on the structure-based sequence alignment function of
360 T_COFFEE/Expresso³⁴ v11.00.8 to perform sequence alignment of the kinase catalytic
361 domain to the templates, followed by the multi-template function of MODELLER³⁵ v9.14
362 to generate 50 homology models covering a range of conformations. For each kinase 10
363 DFG-out models with largest binding site volume, as calculated by POVME³⁶ v2.0, were
364 used for further study. These ensembles of models were evaluated and confirmed to en-
365 rich known type-II inhibitors over non-ligands using docking, which provides an approxi-
366 mation of the binding site flexibility, as well as optimizes the binding site for protein-ligand
367 complementarity and structure-based virtual screening^{11, 26, 37}. The area-under-curve
368 (AUC) of targets BRAF and RET DFG-out models are 90.6 vs. 82.8, respectively, which
369 correspond to at least 5-fold increase in the enrichment accuracy over randomly selected
370 ligands in a known sample set^{37, 38, 39}.

371 **Virtual screening.** Initial virtual screening utilized the ZINC12²¹ “available now” lead-like
372 chemical library (downloaded in 2013, 2.2 million compounds). Default settings were used
373 for the ligand conformer generation with OMEGA and the docking program FRED⁴⁰. For
374 each kinase, the ensemble of 10 DFG-out models was used for screening and the results
375 were processed with the open-source cheminformatics toolkit RDKit (www.rdkit.org). To
376 obtain a consensus docking result for RET and the targets BRAF, SRC, p70-S6K, a two-
377 step approach was used: 1) 2,000 ligands were collected for each kinase by identifying
378 ligands that ranked in the top 10% for at least half of the DFG-out ensemble.; 2) ligands
379 that scored in the top 25% in at least 3 of 4 kinase ensembles were collated into a final
380 set of 247 compounds. These consensus ligands, representing 0.0114% of the library,
381 were visually inspected to remove molecules with energetically unfavorable or strained
382 conformations, or with reactive functional groups that may interfere with assays⁴¹, which
383 are commonly observed in large virtual screenings. 8 compounds were selected based

384 on their interactions with the receptor (DFG-pocket occupancy, hydrogen-bond to con-
385 served amino acids, etc) and chemical novelty and were purchased for *Drosophila* viabil-
386 ity screening. Analogs **1-1**, **1-2**, **2-1 to 2-5**, and others (Table S1) were identified based
387 on the structure of compounds **1** and **2** through the chemical similarity search function
388 available in ZINC15⁸ and SciFinder using the default setting and Tanimoto coefficient
389 above 70%. These compounds are commercially available through vendors such as
390 ChemBridge and Enamine.

391 **Chemical Methods.** For synthetic procedures and characterization data related to com-
392 pounds **1**, **3**, and **4**, please see supplementary materials.

393 **Kinase profiling of compounds.** Kinase inhibition profile of the compounds was as-
394 sessed at 50 μ M through commercially available kinase profiling services (DiscoverX).

395 **Drosophila stocks.** Human orthologs of *Drosophila* genes were predicted by DIOPT
396 (http://www.flyrnai.org/cgi-bin/DRSC_orthologs.pl). The multiple endocrine neoplasia
397 (MEN) type 2B mutant form of *Drosophila* Ret carries the M955T mutation (dRet^{M955T}),
398 which corresponds to the M918T mutation found in human MTC patients. The *ptc-gal4*,
399 *UAS-GFP; UAS-dRet^{M955T}/SM5(tub-gal80)-TM6B* transgenic flies were prepared accord-
400 ing to standard protocols¹⁵. In these flies, the *tubulin* promoter drives GAL80, a suppres-
401 sor of GAL4, to repress dRet^{M955T} expression. We crossed them with *w* flies to obtain
402 *ptc>dRet^{M955T}* flies that lost *GAL80* allele, which derepressed dRet^{M955T} expression (Fig.
403 S1A). Transgenic *ptc>Ret^{M955T}* flies were calibrated to have 0% survival when raised at
404 25°C, which allowed for drug screening (Fig. S1B).

405 **Chemical genetic screening in flies.** We employed dominant modifier screening¹⁵ using
406 the *ptc-gal4, UAS-GFP; UAS-dRet^{M955T}/SM5(tub-gal80)-TM6B* to screen for fly kinase
407 genes that affected the dRet^{M955T}-induced lethality in flies when heterozygous
408 (*ptc>Ret^{M955T};kinase^{-/+}*). Genes that improved or reduced survival of *ptc>dRet^{M955T}* flies
409 when heterozygous were designated as genetic ‘suppressors’ or ‘enhancers’, respec-
410 tively (Fig. 1B). Suppressors are candidate therapeutic targets that when inhibited may
411 reduce tumor progression.

412 Stock solutions of the test compounds were created by dissolving the compound in DMSO
413 at the maximum concentration. The stock solutions were diluted by 1000-fold or more and

414 mixed with semi-defined fly medium (Bloomington Drosophila Stock Center) to make
415 drug-infused food (0.1% final DMSO concentration; maximum tolerable dose in flies). Ap-
416 proximately 100 *ptc>dRet^{M955T}* embryos alongside with wild-type (+;+/SM5_{tubgal80-TM6B})
417 flies were raised until adulthood on drug-infused food for 13 days at 25°C. The numbers
418 of empty pupal cases (*P* in Fig. S1B) and that of surviving adults (*A*) were used to deter-
419 mine percentage of viability, while their body size, which is affected by food intake, tem-
420 perature, and humidity, were compared to vehicle-treated groups to standardize the ex-
421 perimental conditions.

422 **Wing discs cell migration/invasion assays.** Third-instar *ptc>dRet^{M955T}* larvae were dis-
423 sected, and developing wing discs were collected, fixed with 4% paraformaldehyde in
424 PBS, and whole-mounted. At least 10 wing discs were analyzed for each treatment. In-
425vasive GFP-labeled *dRet^{M955T}*-expressing cells were visualized by their green pseudo-
426 color under a confocal microscope. The apical and the virtual z-series views of the wing
427 disc were examined to identify abnormal tissue growth and *dRet^{M955T}*-expressing cells
428 migrating beyond the *ptc* domain boundary.

429

430

431 **ACKNOWLEDGEMENTS**

432 We thank Peter Smibert (New York Genome Center) for *ptc>dRet^{M955T}* flies, Kevin
433 Cook (Bloomington *Drosophila* Stock Center) for kinome mutant fly lines. This work was
434 supported by the National Institutes of Health (R01-GM108911) to A.S. and P.M.U.U. A.S.
435 was also supported by Department of Defense grant W81XWH-15-1-0539. M.S. and R.C.
436 were supported by National Institutes of Health grants U54OD020353, R01-CA170495,
437 and R01-CA109730 and Department of Defense grant W81XWH-15-1-0111. The Dar la-
438 boratory (A.P.S. and A.C.D.) is supported by Innovation awards from the NIH (DP2
439 CA186570-01) and Damon Runyon-Rachleff Foundation. A.C.D. is a Pew-Stewart
440 Scholar in Cancer Research and Young Investigator of the Pershing-Square Sohn Can-
441 cer Research Alliance. We appreciate OpenEye Scientific Software, Inc. for granting us
442 access to its high-performance molecular modeling applications through its academic li-
443 cense program. This work was supported in part through the computational resources
444 and staff expertise provided by the Department of Scientific Computing at the Icahn
445 School of Medicine at Mount Sinai.

446

447 **AUTHOR CONTRIBUTIONS**

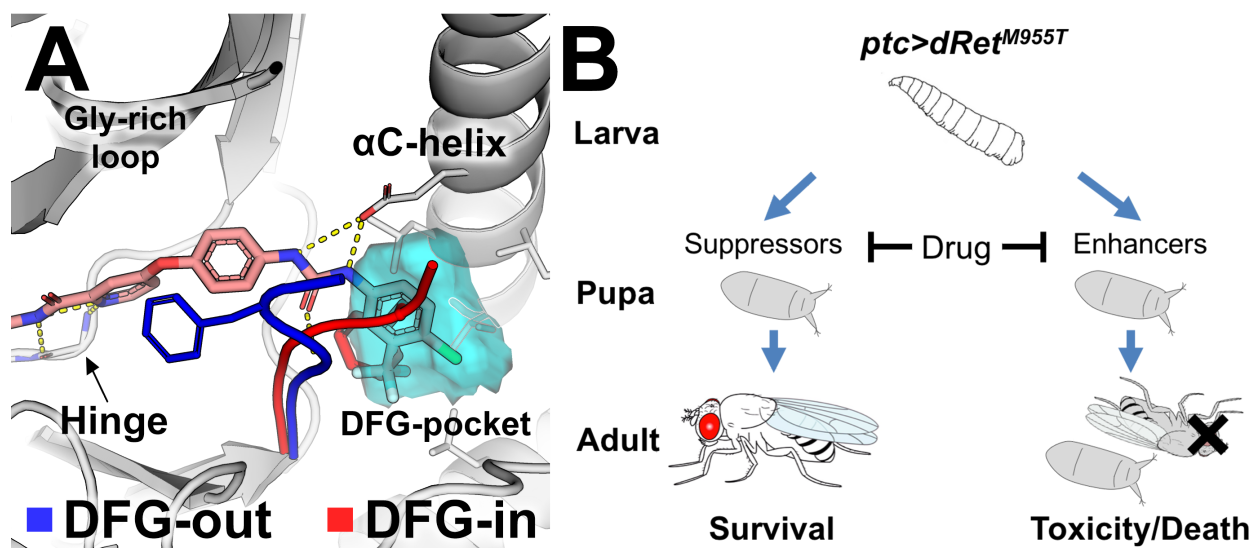
448 P.M.U.U. performed and analyzed the homology modeling of kinases, virtual screening
449 of compound library, selection and design of testing compounds. M.S. managed *Drosoph-*
450 *ila* stocks and testing compounds in whole animal and *in vivo* experiments. A.P.S. con-
451 ducted organic synthesis, design, and validation of test compounds. P.M.U.U. analyzed
452 results and wrote the manuscript with input from all co-authors. R.L.C., A.C.D., and A.S.
453 initiated, supervised, and acquired funding and resources for the project.

454

455 **COMPETING FINANCIAL INTERESTS**

456 None.

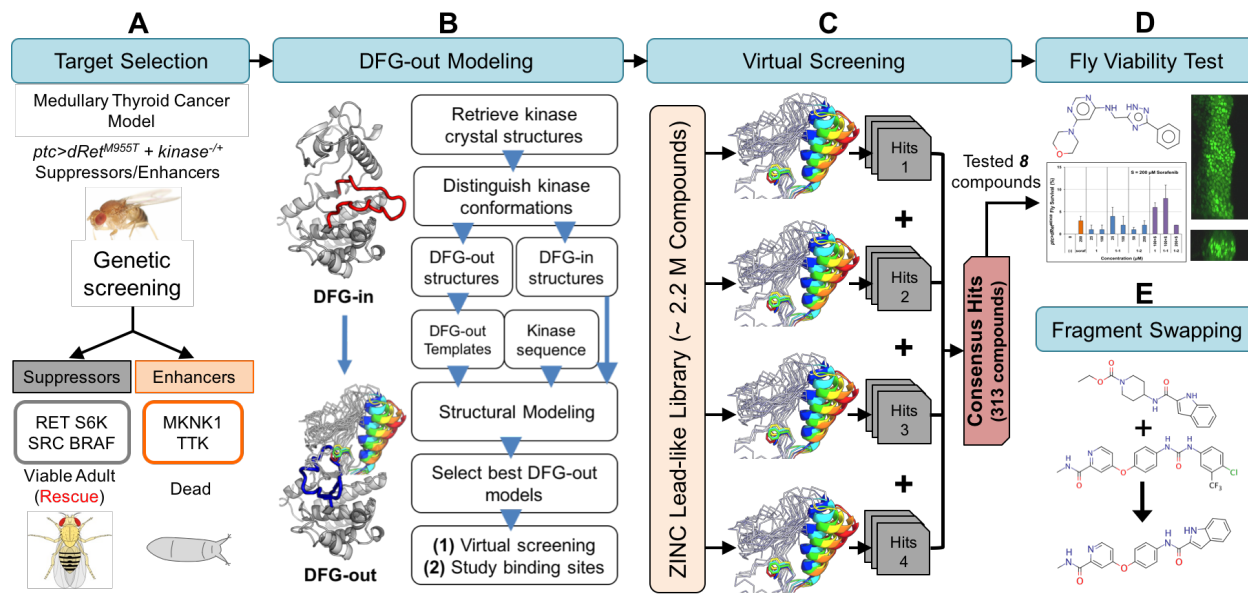
457 **FIGURE LEGENDS**



458
459 **Figure 1. Kinase binding to type-II kinase inhibitors. (A)** The conformational state of
460 protein kinases (e.g., KDR) including DFG-in (red) and DFG-out (blue) is determined by
461 the DFG-motif. The DFG-pocket (cyan mesh) is unique to the DFG-out conformation.
462 Sorafenib is shown in pink. Broken yellow lines indicate hydrogen bonds. **(B)** A scheme
463 depicting the positive and negative effects of drug acting on genetic modifiers of medullary
464 thyroid cancer in a *Drosophila* model. *ptc*-driven *dRet^{M955T}* induces lethality during devel-
465 opment. ‘Suppressors’ or ‘enhancers’ suppress or enhance, respectively, *dRet^{M955T}*-in-
466 duced disease phenotypes as revealed in genetic screening. A drug can suppress lethali-
467 ty by inhibiting the suppressors. It can also induce toxicity and/or worsen transformed
468 phenotypes by inhibiting the enhancers, which results in enhanced lethality.

469

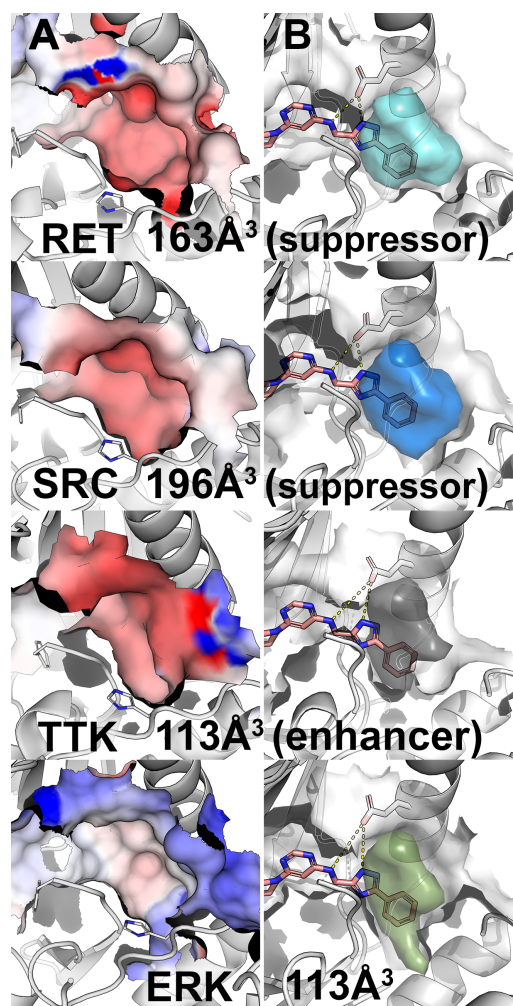
470



471
 472 **Figure 2. Fly genetics and computational chemistry discovery platform.** Key steps
 473 include **(A)** determining suppressors and enhancers in a dominant modifier genetic
 474 screening and their *in silico* modelability, **(B)** generating DFG-out kinase models using
 475 DFGmodel, **(C)** virtual screenings of compound libraries against the modeled suppressors
 476 and enhancers, combining top-ranking screening results into consensus result, **(D)** test-
 477 ing top-ranking compounds for rescue of lethality (left panel) and migration of transformed
 478 cells in developing wing discs of *ptc>dRet^{M955T}* flies (right panel), and **(E)** refining hits by
 479 combining structural elements of computationally derived hits and that of drugs and eval-
 480 uating new targets.

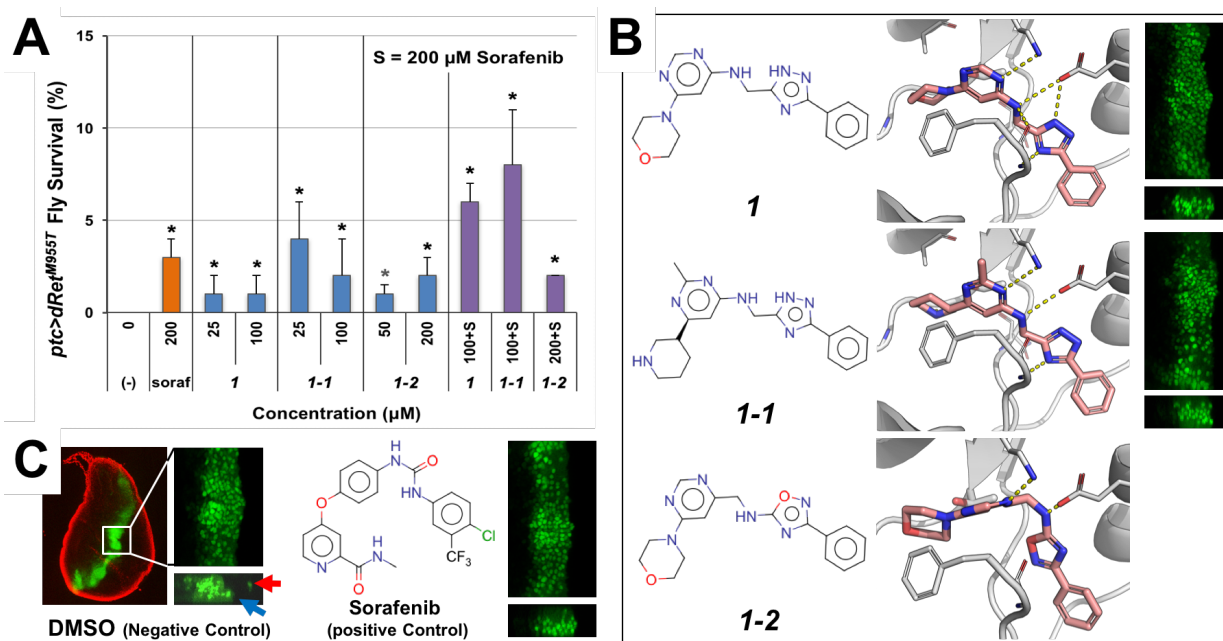
481

482



483
484 **Figure 3. Visualization of DFG-pockets. (A)** Electrostatic potential (red, negative po-
485 tential; blue, positive potential) on the surface of the DFG-pocket in various kinases, in-
486 cluding the suppressors RET and SRC, the enhancer TTK, and ERK. **(B)** Accessible vol-
487 ume of the DFG-pocket (colored volume) for potential type-II kinase inhibitor. Hit molecule
488 **1** is depicted in pink sticks. Broken yellow lines indicate hydrogen bonds.

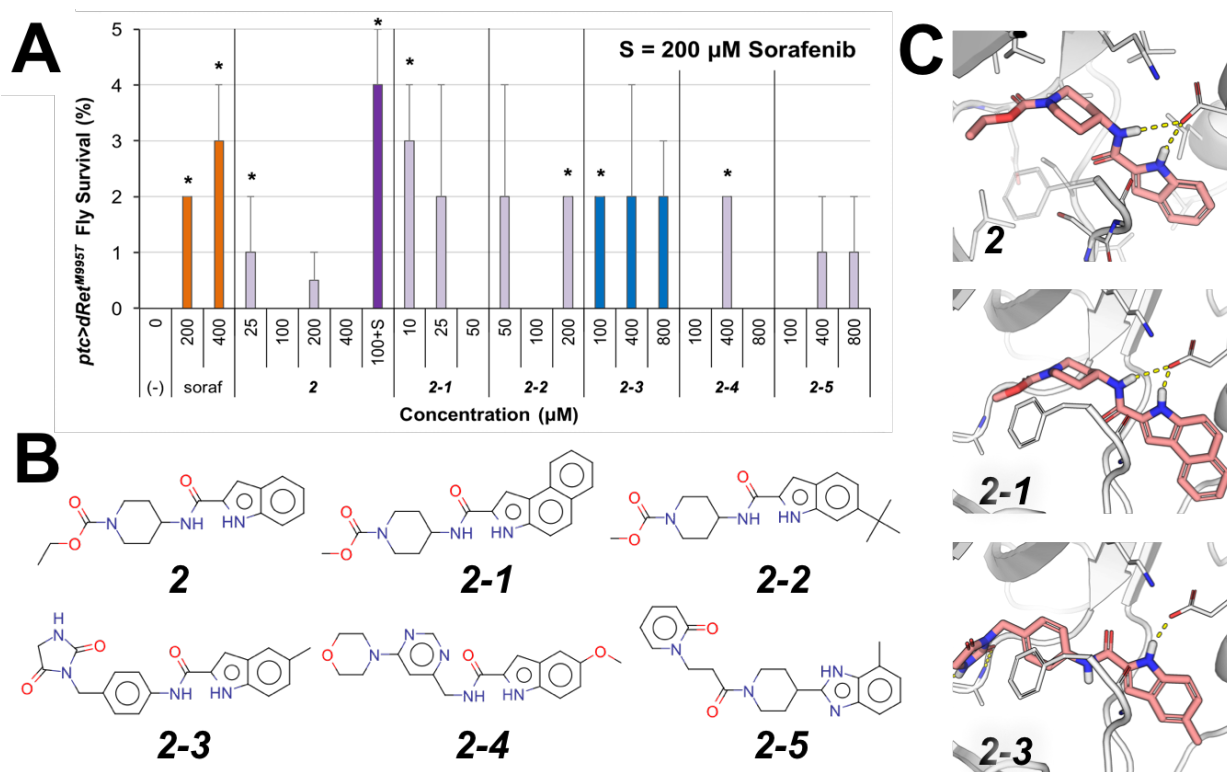
489
490



491
 492 **Figure 4. Compound 1 and its analogs. (A)** Rescue of *ptc>dRet*^{M955T} fly lethality by **1**
 493 and **1-1**. Both showed improved efficacy (synergy) when co-administrated with 200 μM
 494 sorafenib (soraf). (-), vehicle DMSO control. Error bars represent standard error in tripli-
 495 cate experiments. **P* < 0.05 in one-sided Student's *t*-test as compared with vehicle con-
 496 trol. **(B)** Docking pose of **1** and its analogs **1-1** and **1-2** (salmon sticks) with a DFG-out
 497 model of RET (broken yellow lines indicate hydrogen bonds), and their inhibition of mi-
 498 gration of the dRet^{M955T}-expressing cells. Right, suppression of cell migration by **1** and **1-**
 499 **1**. Controls are shown in **(C)**. **(C)** *In vivo* cell migration assay in *ptc>dRet*^{M955T} flies. Left,
 500 a developing whole wing disc containing GFP-labeled, dRet^{M955T}-expressing cells consti-
 501 tuting a stripe in the midline. The disc margin is visualized with DAPI (red pseudocolor).
 502 There are wild-type cells in black areas. Center, overgrowth of dRet^{M955T}-expressing cells
 503 resulting in the thickening of the stripe in the apical view (top). In the z-series view (bot-
 504 tom), dRet^{M955T}-expressing cells are migrating away from the original domain (arrows).
 505 Right, sorafenib suppressed the migration.

506

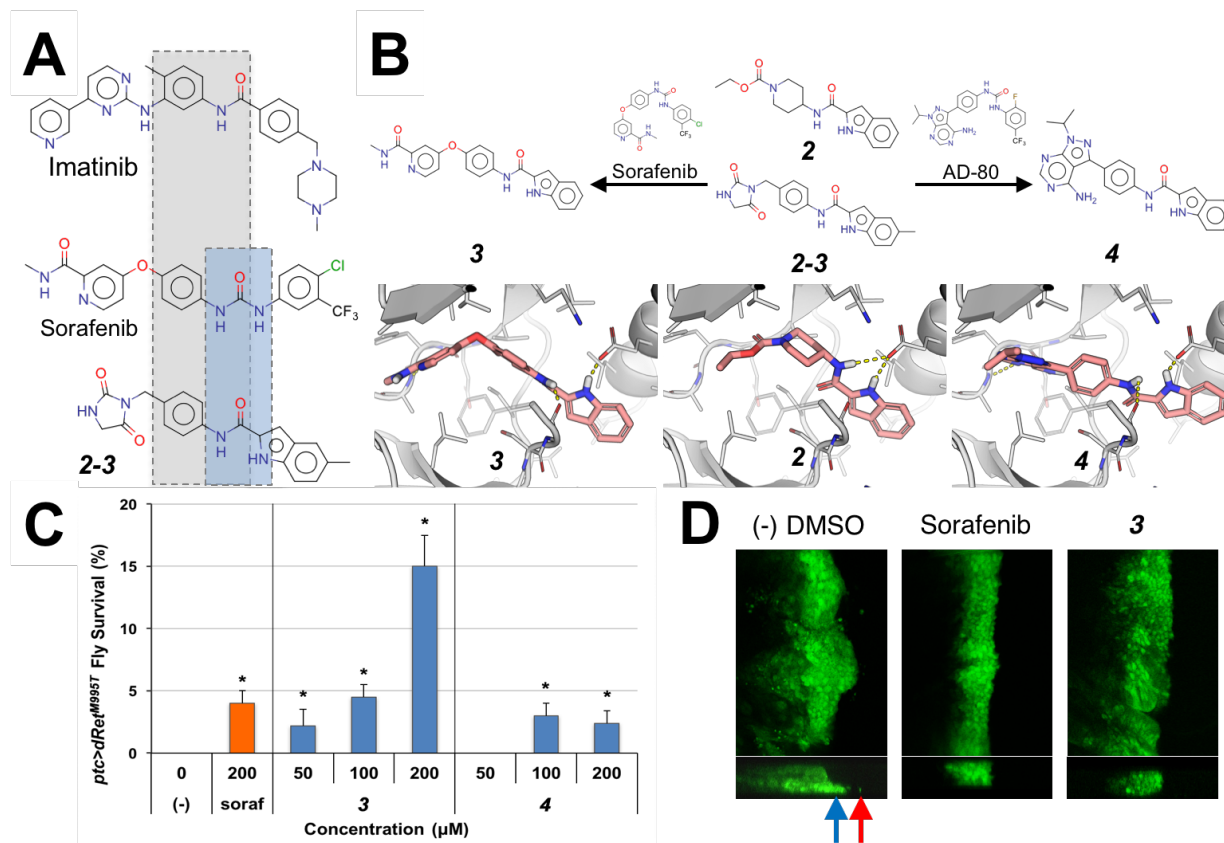
507



508
 509 **Figure 5. Rescue of *ptc>dRet^{M955T}* flies by **2** and its analogs. (A) *ptc>dRet^{M955T}* viabil-**
 510 **ity assay. **2** showed increased efficacy when co-administrated with 200 μM sorafenib. (-**
 511 **), vehicle control. Error bars represent standard error in triplicate experiments. **P* < 0.05**
 512 **in one-sided Student's *t*-test as compared with no-drug control. (B) Chemical structure of**
 513 ****2** and its analogs. (C) Docking pose of **2** and its analogs in a RET DFG-out model. These**
 514 **compounds are proposed to be putative type-II kinase inhibitors that bind in the DFG-**
 515 **pocket through their 1*H*-indole moiety and interact with the conserved αC-helix glutamate**
 516 **side chain and DFG-Aspartate backbone (broken yellow lines).**

517

518



519
 520 **Figure 6. Hybrid compounds with improved efficacy.** (A) The kinase inhibitors
 521 imatinib, sorafenib, and **2-3** share the common *N*-phenylcarboxamide moiety (grey box),
 522 while the *1H*-indole-2-carboxamide of **2-3** resembles the urea linker of sorafenib (blue
 523 box). (B) Hybridization of **2** and sorafenib and AD-80 yielded **3** and **4**, respectively. Top,
 524 chemical structures of compounds. Bottom, docking poses of compounds in a RET DFG-
 525 out model. (C) **3** rescued *ptc>dRet^{M955T}* flies more effectively than by either **2** or sorafenib
 526 alone. (-), vehicle control. Error bars represent standard error in triplicate experiments. **P*
 527 < 0.05 in one-sided Student's *t*-test as compared with no-drug control. (D) **3** suppresses
 528 migration of *dRet^{M955T}*-expressing wing disc cells from the original domain (green) simi-
 529 larly to the positive control, sorafenib. Top and bottom, apical and z-series views, respec-
 530 tively. Arrows, migrating cells.

531

532

533 **TABLES**

534

Table 1. Kinase inhibition profile of compound **1** at 50 μ M.

Kinase	% Inhib.	Kinase	% Inhib.
ABL1	0	mTOR	4
AURKA	22	PDGFRB	21
AURKB	7	RET	15
AURKC	2	RET (M918T)	28
BRAF	9	RET (V804L)	35
CSF1R	3	S6K1	0
FGFR	0	SRC	5
FLT3	52	TTK	17

535 Bold, inhibited by more than 40%.

536

Table 2. Kinase inhibition profile of compounds **2** and **2-3** at 50 μ M.

Compound 2				Compound 2-3			
Kinase	% Inhib.	Kinase	% Inhib.	Kinase	% Inhib.	Kinase	% Inhib.
ABL1	0	mTOR	5	ABL1	2	mTOR	8
AURKA	10	PDGFRB	20	AURKA	13	PDGFRB	91
AURKB	2	RET	34	AURKB	22	RET	24
AURKC	22	RET (M918T)	44	AURKC	2	RET (M918T)	23
BRAF	0	RET (V804L)	44	BRAF	0	RET (V804L)	43
CSF1R	12	S6K1	0	CSF1R	20	S6K1	0
FGFR	0	SRC	6	FGFR	4	SRC	0
FLT3	25	TTK	31	FLT3	78	TTK	26

537 Bold, inhibited by more than 40%.

538

539

Table 3. Kinase inhibition profile of compound **3** at 50 μ M.

Kinase	% Inhib.	Kinase	% Inhib.
ABL1	0	mTOR	4
AURKA	15	PDGFRB	98
AURKB	88	RET	29
AURKC	91	RET (M918T)	26
BRAF	4	RET (V804L)	46
CSF1R	95	S6K1	0
FGFR	0	SRC	4
FLT3	80	TTK	27

540 Bold, inhibited by more than 40%.

541

542 **REFERENCES**

- 543 1. Dar AC, Das TK, Shokat KM, Cagan RL. Chemical genetic discovery of targets
544 and anti-targets for cancer polypharmacology. *Nature* **486**, 80-84 (2012).
545
- 546 2. Kasai Y, Cagan R. Drosophila as a tool for personalized medicine: a primer.
547 *Personalized medicine* **7**, 621-632 (2010).
548
- 549 3. Sonoshita M, Cagan RL. Modeling Human Cancers in Drosophila. *Curr Top Dev*
550 *Biol* **121**, 287-309 (2017).
551
- 552 4. Vidal M, Wells S, Ryan A, Cagan R. ZD6474 suppresses oncogenic RET isoforms
553 in a Drosophila model for type 2 multiple endocrine neoplasia syndromes and
554 papillary thyroid carcinoma. *Cancer research* **65**, 3538-3541 (2005).
555
- 556 5. Manning G, Whyte DB, Martinez R, Hunter T, Sudarsanam S. The protein kinase
557 complement of the human genome. *Science* **298**, 1912-1934 (2002).
558
- 559 6. Read RD, Goodfellow PJ, Mardis ER, Novak N, Armstrong JR, Cagan RL. A
560 Drosophila model of multiple endocrine neoplasia type 2. *Genetics* **171**, 1057-1081
561 (2005).
562
- 563 7. Schlessinger A, Abagyan R, Carlson HA, Dang KK, Guinney J, Cagan RL. Multi-
564 targeting Drug Community Challenge. *Cell Chem Biol* **24**, 1434-1435 (2017).
565
- 566 8. Sterling T, Irwin JJ. ZINC 15--Ligand Discovery for Everyone. *Journal of chemical*
567 *information and modeling* **55**, 2324-2337 (2015).
568
- 569 9. Irwin JJ, Shoichet BK. Docking Screens for Novel Ligands Conferring New Biology.
570 *Journal of medicinal chemistry* **59**, 4103-4120 (2016).
571
- 572 10. Ung PMU, Schlessinger A. DFGmodel: predicting protein kinase structures in
573 inactive states for structure-based discovery of type-II inhibitors. *ACS chemical*
574 *biology* **10**, 269-278 (2015).
575
- 576 11. Abagyan R, *et al.* Accurate ligand docking and screening: Lessons from the
577 Pocketome. *Abstr Pap Am Chem S* **245**, (2013).
578
- 579 12. Cerrato A, De Falco V, Santoro M. Molecular genetics of medullary thyroid
580 carcinoma: the quest for novel therapeutic targets. *Journal of molecular*
581 *endocrinology* **43**, 143-155 (2009).
582
- 583 13. Hadoux J, Pacini F, Tuttle RM, Schlumberger M. Management of advanced
584 medullary thyroid cancer. *The lancet Diabetes & endocrinology* **4**, 64-71 (2016).
585

- 586 14. Vidal M, Larson DE, Cagan RL. Csk-deficient boundary cells are eliminated from
587 normal *Drosophila* epithelia by exclusion, migration, and apoptosis.
588 *Developmental cell* **10**, 33-44 (2006).
589
- 590 15. Sonoshita M, *et al.* A whole-animal platform to advance a clinical kinase inhibitor
591 into new disease space. *Nature chemical biology* **14**, 291-298 (2018).
592
- 593 16. Wan PT, *et al.* Mechanism of activation of the RAF-ERK signaling pathway by
594 oncogenic mutations of B-RAF. *Cell* **116**, 855-867 (2004).
595
- 596 17. Seeliger MA, Nagar B, Frank F, Cao X, Henderson MN, Kuriyan J. c-Src binds to
597 the cancer drug imatinib with an inactive Abl/c-Kit conformation and a distributed
598 thermodynamic penalty. *Structure* **15**, 299-311 (2007).
599
- 600 18. Huse M, Kuriyan J. The conformational plasticity of protein kinases. *Cell* **109**, 275-
601 282 (2002).
602
- 603 19. Zhao Z, *et al.* Exploration of type II binding mode: A privileged approach for kinase
604 inhibitor focused drug discovery? *ACS chemical biology* **9**, 1230-1241 (2014).
605
- 606 20. Mulligan LM. RET revisited: expanding the oncogenic portfolio. *Nature reviews*
607 *Cancer* **14**, 173-186 (2014).
608
- 609 21. Irwin JJ, Sterling T, Mysinger MM, Bolstad ES, Coleman RG. ZINC: a free tool to
610 discover chemistry for biology. *Journal of chemical information and modeling* **52**,
611 1757-1768 (2012).
612
- 613 22. Scholl C, Gilliland DG, Frohling S. Deregulation of signaling pathways in acute
614 myeloid leukemia. *Semin Oncol* **35**, 336-345 (2008).
615
- 616 23. Keiser MJ, Roth BL, Armbruster BN, Ernsberger P, Irwin JJ, Shoichet BK. Relating
617 protein pharmacology by ligand chemistry. *Nat Biotechnol* **25**, 197-206 (2007).
618
- 619 24. Schlessinger J. Cell signaling by receptor tyrosine kinases. *Cell* **103**, 211-225
620 (2000).
621
- 622 25. Burchat A, Borhani DW, Calderwood DJ, Hirst GC, Li B, Stachlewitz RF. Discovery
623 of A-770041, a src-family selective orally active lck inhibitor that prevents organ
624 allograft rejection. *Bioorganic & medicinal chemistry letters* **16**, 118-122 (2006).
625
- 626 26. Amaro RE, Li WW. Emerging methods for ensemble-based virtual screening. *Curr*
627 *Top Med Chem* **10**, 3-13 (2010).
628
- 629 27. Vidal M, Warner S, Read R, Cagan RL. Differing Src signaling levels have distinct
630 outcomes in *Drosophila*. *Cancer research* **67**, 10278-10285 (2007).
631

- 632 28. Sachsenmaier C, Sadowski HB, Cooper JA. STAT activation by the PDGF
633 receptor requires juxtamembrane phosphorylation sites but not Src tyrosine kinase
634 activation. *Oncogene* **18**, 3583-3592 (1999).
635
- 636 29. Sasai K, *et al.* Aurora-C kinase is a novel chromosomal passenger protein that can
637 complement Aurora-B kinase function in mitotic cells. *Cell Motil Cytoskeleton* **59**,
638 249-263 (2004).
639
- 640 30. Baldini E, *et al.* Aurora kinases are expressed in medullary thyroid carcinoma
641 (MTC) and their inhibition suppresses in vitro growth and tumorigenicity of the MTC
642 derived cell line TT. *BMC Cancer* **11**, 411 (2011).
643
- 644 31. Tuccilli C, *et al.* Preclinical testing of selective Aurora kinase inhibitors on a
645 medullary thyroid carcinoma-derived cell line. *Endocrine* **52**, 287-295 (2016).
646
- 647 32. Bavetsias V, Linardopoulos S. Aurora Kinase Inhibitors: Current Status and
648 Outlook. *Front Oncol* **5**, 278 (2015).
649
- 650 33. Grundy M, Seedhouse C, Shang S, Richardson J, Russell N, Pallis M. The FLT3
651 internal tandem duplication mutation is a secondary target of the aurora B kinase
652 inhibitor AZD1152-HQPA in acute myelogenous leukemia cells. *Mol Cancer Ther*
653 **9**, 661-672 (2010).
654
- 655 34. Notredame C, Higgins DG, Heringa J. T-Coffee: A novel method for fast and
656 accurate multiple sequence alignment. *Journal of molecular biology* **302**, 205-217
657 (2000).
658
- 659 35. Sali A, Blundell TL. Comparative protein modelling by satisfaction of spatial
660 restraints. *Journal of molecular biology* **234**, 779-815 (1993).
661
- 662 36. Durrant JD, Votapka L, Sorensen J, Amaro RE. POVME 2.0: An Enhanced Tool
663 for Determining Pocket Shape and Volume Characteristics. *Journal of chemical*
664 *theory and computation* **10**, 5047-5056 (2014).
665
- 666 37. Fan H, Irwin JJ, Webb BM, Klebe G, Shoichet BK, Sali A. Molecular docking
667 screens using comparative models of proteins. *Journal of chemical information and*
668 *modeling* **49**, 2512-2527 (2009).
669
- 670 38. Katritch V, Rueda M, Lam PC, Yeager M, Abagyan R. GPCR 3D homology models
671 for ligand screening: lessons learned from blind predictions of adenosine A2a
672 receptor complex. *Proteins* **78**, 197-211 (2010).
673
- 674 39. Carlsson J, *et al.* Ligand discovery from a dopamine D3 receptor homology model
675 and crystal structure. *Nature chemical biology* **7**, 769-778 (2011).
676
- 677 40. OEDOCKING 3.2.0.2: OpenEye Scientific Software, Santa Fe, ME. (ed^(eds).

- 678
679 41. Baell JB, Holloway GA. New substructure filters for removal of pan assay
680 interference compounds (PAINS) from screening libraries and for their exclusion
681 in bioassays. *Journal of medicinal chemistry* **53**, 2719-2740 (2010).
682

683